Plasmonic Coupled Modes in a Metal-Dielectric Periodic Nanostructure

Victor Coello , Mas-ud Ayodeji Abdulkareem , César Eduardo García Ortíz * , Citlalli Teresa Sosa-Sánchez , Ricardo Téllez-Limón , Marycarmen Peña-Gomar

Posted Date: 14 July 2023

doi: 10.20944/preprints202307.1002.v1

Keywords: plasmonics; metasurfaces; gap surface plasmons; surface lattice resonances

Article

Plasmonic Coupled Modes in a Metal-Dielectric Periodic Nanostructure

Victor Coello [1], Mas-ud A. Abdulkareem [2], Cesar E. Garcia-Ortiz [3,*], Citlalli T. Sosa-Sánchez [1], Ricardo Téllez-Limón [4] and Marycarmen Peña-Gomar [2]

[1] Centro de Investigación Científica y de Educación Superior de Ensenada, Unidad Monterrey, Alianza Centro 504, PIIT, Apodaca 66629, Mexico; csosa@cicese.mx
[2] Universidad Michoacana de San Nicolás de Hidalgo, Avenida Francisco J. Múgica s/n, Ciudad Universitaria C. P. 58030, Morelia Mich., Mexico; kareemmasud@yahoo.com (M.A.A.); mgomar@umich.mx (M.P.-G.)
[3] Tecnologico de Monterrey, School of Engineering and Sciences, Monterrey NL 64849, Mexico
[4] CONACYT - Centro de Investigación Científica y de Educación Superior de Ensenada, Unidad Monterrey, Alianza Centro 504, PIIT, Apodaca 66629, Mexico; rtellez@cicese.mx
* Correspondence: cegarciaor@tec.mx

Abstract: We report on a 2D-gap surface plasmon metasurface based composed of a bottom metal layer, middle insulator layer, and top metal nanostructure of gold nanoblocks (nanoantennas). The proposed structure enables us to generate simultaneous multi plasmonic resonances and offers the possibility to tune them, within the near-infrared domain. The simplicity of the metasurface makes it promising for compact optical platforms based on reflection mode operation with potential application in multi-channel biosensors, second-harmonic generation, and multi-wavelength surface-enhanced spectroscopy among other interesting fields.

Keywords: plasmonics; metasurfaces; gap surface plasmons; surface lattice resonances

1. Introduction

Periodic arrays of plasmonic nanoparticles [1–3] are essential structures in nanoscience and nanotechnology and therefore, a deep understanding of their fundamental properties and applications is necessary for the development of advanced nanophotonic circuitry [4–6]. Unlike the metal-dielectric interface, which only supports well-known surface plasmon polaritons (SPPs) [7,8] and localized surface plasmons (LSPs), such arrays can couple modes between the LSP of a single constituent scatterer (typically a nanoparticle) and the diffractive modes of the lattice structure, resulting in particle-lattice field enhancements larger than those of the same number of isolated elements [11–13]. Such coupled electromagnetic modes are referred to as surface lattice resonances (SLRs) [2,14], and their optical properties are highly dependent on the lattice periodicity, scatterer morphology, nature of the metal, and the refractive index of the environment. Properly designed periodic nanoparticle arrays can control plasmonic dispersion curves [15,16], obtain exceptionally high-Q resonances [17], and achieve subwavelength control of nano-optical fields [18,19]. Examples of such designs include nano-antennas [20], waveguides [21,22], metalenses [18,23], and nanocavities [24]. However, achieving precise control of hybridized plasmonic resonances is challenging due to the relatively high number of parameters involved in an SLR coupled system. In this context, gap surface plasmon metasurfaces (GSPMs) [25] based on metal-insulator-metal (MIM) nanostructures [26] have exhibited strong broadband absorption of multi-spectral coverage. The thickness of the dielectric function of the sandwiched material closely correlates with such absorption [27], and this geometry has also shown excellent performance in optical phase, amplitude, and polarization manipulation of reflected fields [28]. In this work, we report on a 2D-GSPM designed to generate simultaneous multi-plasmonic resonances, with the possibility to tune them within the near-infrared domain. Reflection spectra of the proposed structure were calculated for different array periods, and

Preprints (www.preprints.org) | NOT PEER-REVIEWED | Posted: 14 July 2023 doi:10.20944/preprints202307.1002.v1

two dips were observed with reflectivity values that nearly reached zero. The broader dip is associated with the GSP effect, and the dips with the smallest bandwidth exhibit a nearly linear dispersion in wavelength when the period of the grid is varied. The resonance associated with the GSP effect is shown to exhibit a blue shift with increasing gap thickness, while a spectral redshift is observed for gap thicknesses larger than 100 nm. We calculated the near field optical distribution around the nanoblocks to gain a deeper understanding of the optical response of the system. This development has potential applications in multi-channel biosensors [29], second-harmonic generation [30], multi-wavelength surface-enhanced spectroscopy [31], and other interesting fields.

2. Materials and Methods

We used the finite difference time domain method (FDTD) to perform an electromagnetic simulation of a GSPM. The FDTD method is a numerical technique used to solve electromagnetic problems by dividing space and time into a finite number of small cells. By applying a such numerical method to the GSPM, we were able to accurately model the electromagnetic interactions within the structure and gain insights into its optical properties. This allowed us to investigate the behavior of the GSPM under different external conditions. The GSPM is composed of three layers: a bottom metal layer, a middle insulator layer, and a top layer consisting of gold nanoblocks (nanoantennas) (Figure 1, b). The sample consists of several structural parameters, including lattice periodicity (Λ), dielectric gap (*t*), nanoblocks length (*L*) and height (*h*), and an infinitely thick metal substrate thickness. To simulate an infinite array, we applied a periodic boundary condition at the walls perpendicular to the unit cell, and a uniaxial anisotropic perfectly matched layer (PML) was applied in the walls parallel. The refractive index of air at room temperature (T=300 K) was used as the background, and the dielectric constants of gold were extrapolated from Johnson and Christy's experimental results [32], while the optical constants of the SiO2 gap were extracted from Palik experimental data [33]. To absorb energy flowing at grazing incidence, we set the number of PML layers to 12. We used a mesh size of (5x5x5) nm^3 in space and (2x2x2) nm^3 around the nanoparticles. The simulation was run with a time step of 0.0095 fs, corresponding to a stability factor of 0.5, and a simulation time of 1500 fs. Finally, we modeled the incident light as a Gaussian wave packet composed of plane waves with the wave vector parallel to the surface and with the electric field polarized along the x-axis (TM polarized) in Figure 1 (a). The incident light was normal to the surface of the structure.

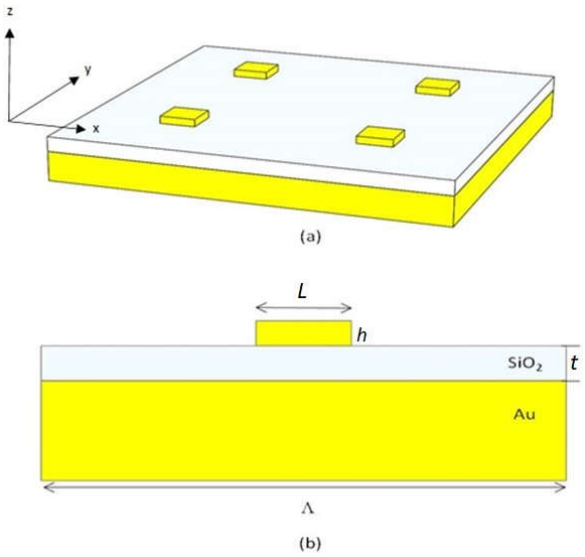

Figure 1. (a) 2D and (b) 1D schematic of the GSP metasurface. It consists of a periodic array of nanoblocks that have been disposed along the surface to scatter light in a controlled manner.

Preprints (www.preprints.org) | NOT PEER-REVIEWED | Posted: 14 July 2023 doi:10.20944/preprints202307.1002.v1

3. Results and discussions

First, we calculated the reflection spectra of the GSPM structure under normal incidence and for different array periods (Figure 2).

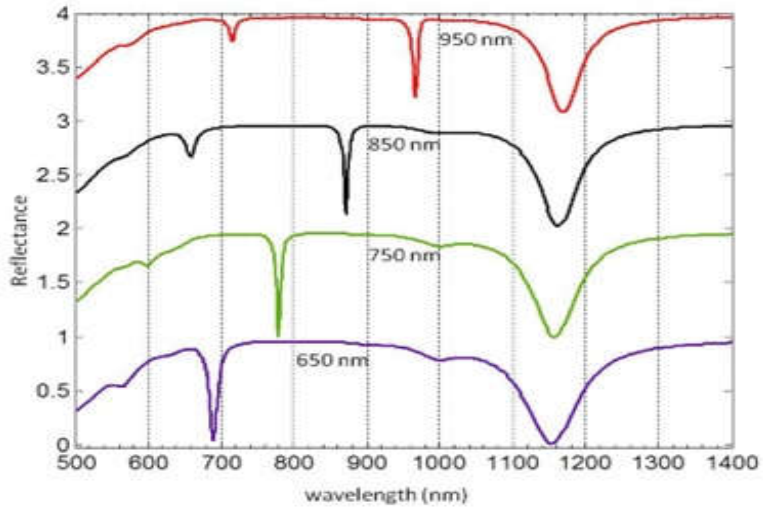

Figure 2. Reflectivity spectra curves for different lattice periods (Λ): 950 (red line) 850 (black line), 750 (green line) and 650 (purple line) nm.

The thickness of the gold film was fixed at 100 nm, which is sufficient to achieve nearly zero optical transmission. The parameters *L* and *h* were set to 200 nm and 50 nm, respectively, while *t* was fixed at 25 nm [Figure 1 (b)]. These parameter values align with those used in experimental studies on light-matter interactions in similar systems, as documented in the literature [34]. Each calculated reflection spectrum exhibited two distinct dips, as depicted in Figure 2. The reflectivity values at these dips approached zero, indicating the presence of resonant modes within the system. Notably, the broader dip at 1150 nm was consistently observed in all calculated spectra, regardless of the array periodicity. This dip was located far from the SPP resonances that could be generated by the grating resonance of the nanoantenna array (i.e., Rayleigh anomalies).

Hence, the origin of the reflection suppression in our GSPM structure can be attributed to a Fano-type hybridization mechanism. This mechanism arises from the spectral overlap between the LSP resonances of the metallic nanoblock and the SPP resonances of the underlying metal layer. As a result of this coupling, a GSP resonance is generated within the system. The GSP mode is localized between the metallic nanoblock and the underlying metal layer, creating a distinct resonant state. This resonance corresponds to specific frequencies or wavelengths at which the system exhibits a significant reduction in reflection.

Consequently, there is a strong field enhancement and confinement in the dielectric region of the gap. GSP modes [25] exhibit broad resonances that are minimally affected by the array periodicity. This behavior arises due to the enhanced near-field coupling between the metal film and the nanoblocks when the gap thickness is much smaller than the wavelength of the incident light. This effect can be understood in the context of a Fabry-Perot resonator [13], which involves multiple reflections between metal surfaces and results in the generation of transmission peaks and reflection dips in the system's spectral response due to interference phenomena between the reflected waves. However, it is important to note that the GSP resonance relies on the interference of surface waves, rather than the interference of waves between two mirrors as in the case of a Fabry-Perot resonator. The detailed mechanism underlying the transition from Fabry-Perot resonance to GSPR falls outside the scope of the present study. Interested readers are referred to relevant literature, including [13] and references therein. On the other hand, the dips with the smallest bandwidth, as shown in Figure 2, exhibit a nearly linear dispersion in wavelength when the lattice period is varied. In all cases, the minimum value of the reflectance spectrum essentially coincides with the period of the grid. When

Preprints (www.preprints.org) | NOT PEER-REVIEWED | Posted: 14 July 2023 doi:10.20944/preprints202307.1002.v1

light is incident on this array, one of the diffracted waves can travel along the surface at a grazing angle and interact with many other nanoantennas. This results in the creation of a mixed (hybrid) mode of LSP vibrations combined with the diffracted grazing wave, leading to an increase in the intensity of the LSP resonances. As a result of this process, the incident beam transfers energy into the LSP modes in a narrow wavelength range near a Wood anomaly [35]. In the case of the nanoantenna array, the Wood anomaly enhances the interaction of the incident light with the LSP modes, producing sharp plasmon resonances.

In addition, we examined the reflectance spectra of a GSPM structure with a constant array period but varying gap thickness, as illustrated in Figure 3.

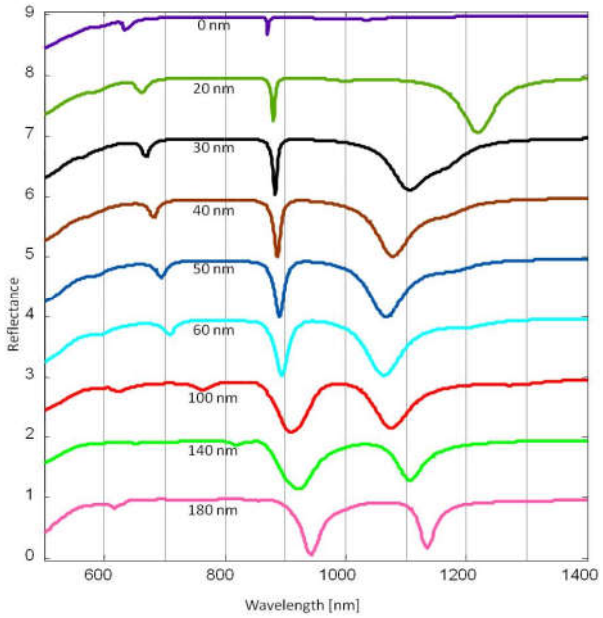

Figure 3. Reflectivity spectra curves for different dielectric gap thicknesses. Λ was fixed to 950 nm.

The results showed that the resonance associated with the GSP effect experienced a blue shift with an increase in gap thickness. This blue shift can be attributed to a decrease in the effective refractive index of the GSP mode as the gap thickness increased. In other words, the change in the effective refractive index of the GSP mode, influenced by the gap thickness, caused the resonance to shift to higher frequencies resulting in the observed blue shift. However, a different trend appears with thicknesses larger than 100 nm where a spectral redshift is observed. It has been mentioned that the physical phenomena that are involved in the generation of SLR are vast. Despite this complexity, it is possible to assume, at least in a general form, that the generation of hybrid plasmonic modes arises mainly from the interaction between localized and delocalized modes, and a mutual combination of them. In this case, the resonance behaviors associated with the diffraction gratings (SPP Bloch modes) and those that have a possible origin in a GSP effect are far apart from each other and then, it is difficult to assume that they are effectively interacting (Figure 3). It is important to note that when the separation between the resonant wavelengths of two SLRs is larger than the linewidth of each resonance, there is negligible or no interaction between them. This phenomenon occurs as a consequence of the limited spectral overlap between the resonances, which is determined by the full width at half maximum (FWHM) of each resonance. It should be noted, however, that the precise criterion for determining whether two SLRs can or cannot interact is dependent on the particular system being considered and the nature of the coupling between the resonances. Another approach to describe this optical response is based on the fact that part of the scattered light can be coupled to SPPs that would exist between neighboring nanoblocks, potentially influencing the SLR of the system. The coupling of scattered light to SPPs between neighboring nanoblocks is a well-known mechanism in plasmonics. However, the extent to which this coupling occurs and its effect on the

Preprints (www.preprints.org) | NOT PEER-REVIEWED | Posted: 14 July 2023 doi:10.20944/preprints202307.1002.v1

SLR of the system depends on several factors such as the geometry, size, and spacing of the nanoblocks, as well as the surrounding dielectric environment.

The complex hybridization effects observed in our results can be better understood by analyzing the dispersion of resonance angles as the periodicity of the nanoblock arrays is varied (Figure 4). When examining the overlap of the LSPs and SLR resonance angles, an anticrossing region becomes evident. This region indicates the hybridization of modes that occur at wavelengths around 1080 nm and share similar periodicities. Within this anticrossing region, the modes exhibit a complex near-field distribution resulting from the coupling of both localized and propagating modes. This coupling gives rise to unique electromagnetic phenomena, leading to enhanced light-matter interactions and intricate energy transfer mechanisms. Calculating the near field zone around the nanoblocks can provide valuable information about the electromagnetic field distribution and can help to better understand the optical response of the system. The near field zone refers to the region in the immediate vicinity of the nanoblocks where the electromagnetic field is strongly influenced by the presence of the nanoblocks. By calculating the near field zone, one can determine the strength and spatial distribution of the electromagnetic field around the nanoblocks, and how it varies with changes in gap size. This information helps to validate the assumption that scattered light can be coupled to SPPs between neighboring nanoblocks, as well as provide insights into other phenomena such as plasmon hybridization and field enhancement (Figure 5). The calculated near-field optical images showed a clear field redistribution (Figure 5) once the gap becomes very large. As the gap increases, the near field coupling tends to be weak and the GSP resonance is hardly supported, therefore, the effects of the SPPs between neighboring nanoblocks will increase causing the spectral redshift.

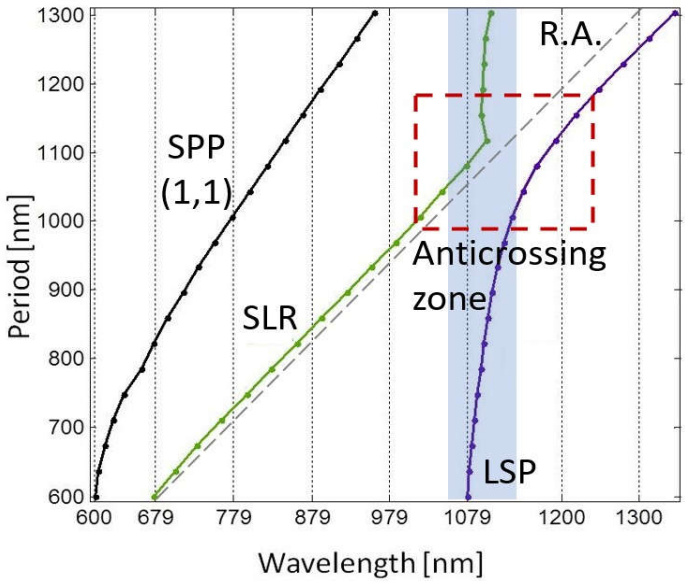

Figure 4. Distribution of resonance wavelengths as a function of the periodicity of the nanoblock arrays. The dispersion shows the presence of SPPs, SLRs, LSP and an anticrossing region indicating the hybridization of localized and propagating modes. The gray dashed line corresponds to the Rayleigh anomaly R.A.

Preprints (www.preprints.org) | NOT PEER-REVIEWED | Posted: 14 July 2023 doi:10.20944/preprints202307.1002.v1

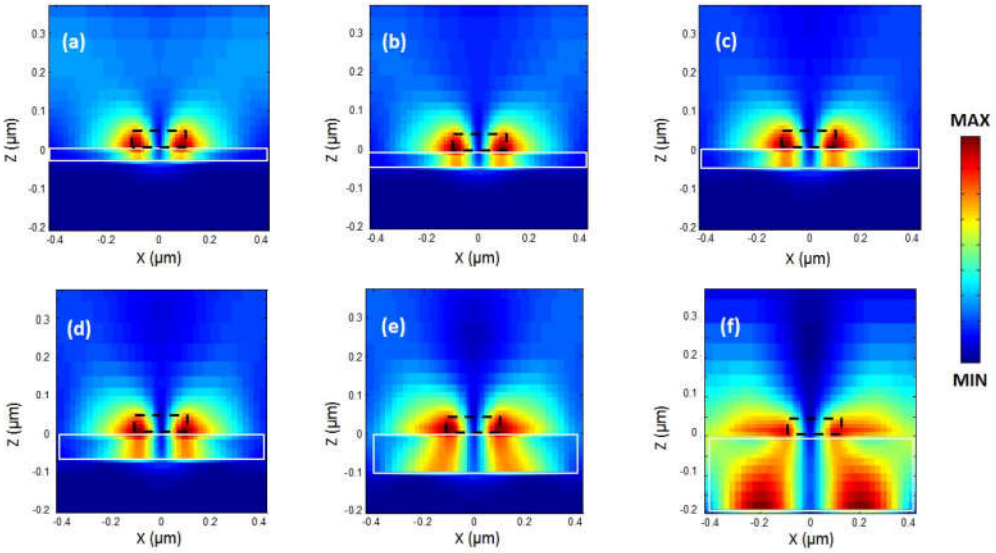

Figure 5. Near-field optical distributions of the resonant electric field magnitude in the (x,z)-plane for different SiO2 layer thicknesses (a) t = 20 nm, (b) t = 30 nm, (c) t= 40 nm, (d) t=50 nm, (e) t= 100, and (f) t=200 nm in a periodic GSPM array with Λ = 860 nm. The dotted (black) and solid (white) lines are to guide the eye and represent the nanoblock and the thickness of the dielectric, respectively.

4. Conclusions

We studied the reflection spectra of a GSPM under normal incidence with x-polarized plane waves. The GSP effect is responsible for the broader dip centered around 1150 nm, being common to all periods and apparently independent of array periodicity. The dips with the smallest bandwidth, exhibit a nearly linear dispersion in wavelength when the period of the grid is varied. These dips are produced by the interaction of the incident light with the LSP modes, producing sharp plasmon resonances. The effective refractive index of the GSP mode changes with the thickness of the gap, resulting in a shift in the resonant frequency. The physical phenomena that are involved in the generation of hybrid plasmonic modes arise mainly from the interaction between localized and delocalized modes, and a mutual combination of them. The exact criterion for determining whether two SLRs can or cannot interact is dependent on the particular system being considered and the nature of the coupling between the resonances. Based on these findings, potential applications for the design and optimization of plasmonic devices can be envisioned. For instance, controlling the spectral behavior of hybrid plasmonic modes through the thickness of the gap can be useful for the development of sensors, filters, and modulators. In addition, understanding the interplay between SLR and GSP modes can aid in the creation of new types of plasmonic structures with unique optical properties. Future work in this area may involve exploring the influence of other parameters on the spectral behavior of hybrid plasmonic modes, such as the material properties of the grating and the dielectric layer, the incident angle and polarization of the light, and the presence of defects or variations in the grating structure. Furthermore, investigating the potential for nonlinear optical effects in hybrid plasmonic modes may be of interest for the development of new types of all-optical switches and logic gates.

Author Contributions: Conceptualization, V.C., C.G, and R.T.-L.; investigation M.A.A., C.G., and V.C.; methodology R.T.L and C.G.; software, C.T.S.-S., and M.A.A.; formal analysis, M.A.A., C.G., and V.C..; writing, V.C., M.A.A., and C.G.; supervision, V.C., C.G., and R.T.-L. All authors have read and agreed to the published version of the manuscript.

Funding: Please add: This research was funded by CICESE, Unidad Foránea Monterrey, internal project 692-103, CONAHCYT Postdoctoral project No. I1200/320/2022, and CONAHCYT CF-2023-I-1464.

Data Availability Statement: The data presented in this study are available on request from the corresponding author.

Conflicts of Interest: The authors declare no conflict of interest.

References

1. Zhen Y-Rong, Fung K H, and Chan C. T. Collective plasmonic modes in two-dimensional periodic arrays of metal nanoparticles. Phys. Rev. B **2008**, 78, 035419-035433.
2. Kravets V.G., Kabashin A.V., Barnes W.L., Grigorenko A.N. Plasmonic Surface Lattice Resonances: A Review of Properties and Applications. Chem. Rev. **2018**, 12, 5912-5951.
3. Kasani S., Curtin K., Wu N. A review of 2D and 3D plasmonic nanostructure array patterns: fabrication, light management and sensing applications. Nanophotonics **2019**, 8, 2065-2089.
4. He J., Paradisanos J.,Liu T., Cadore A.R., Liu J., Churaev M., Wang R.N., Raja A.S., Javerzac-Galy C., Roelli P., De Fazio D., Rosa B., Tongay S., Soavi G., Ferrari A.C., and Kippenberg T.J. Low-Loss Integrated Nanophotonic Circuits with Layered Semiconductor Materials. Nano Lett **2021,** 21, 2709-2718.
5. Ma P., Gao L., Ginzburg P., and Nosko R.E. Nonlinear Nanophotonic Circuitry: Tristable and Astable Multivibrators and Chaos Generator. Laser Photonics Rev. **2020**, 14 1900304- 900313.
6. Shen Y., Harris C.N., Skirlo S., Prabhu M., Baehr-Jones T., Hochberg M., Sun X., Zhao S., Larochelle H., Englund D., and Soljačić M. Deep learning with coherent nanophotonic circuits. Nature **2017**, 11 441-446.
7. Zayats A.V., Smolyaninov I. I., Maradudin A.A. Nano-optics of surface plasmon polaritons. Phys. Rep. **2005** 408 131-314.
8. Bozhevolnyi. S. I. and Coello V. Elastic scattering of surface plasmon polaritons: Modeling and experiment. **1998** 58 10899-10910.
9. Petryayeva E., and Krull U.J. Localized surface plasmon resonance: Nanostructures, bioassays and biosensing—A review. Analytica Chimica Acta **2011**, 706 8-24.
10. Mayer M.K. and Hafner J.H. Localized Surface Plasmon Resonance Sensors. Chem. Rev. **2011**, 111 3828-3857.
11. Klarskov P., Tarekegne A.T., Iwaszczuk K., Zhang X.-C., and Jepsen P.U. Amplification of resonant field enhancement by plasmonic lattice coupling in metallic slit arrays. Sci. Rep. **2016**, 6 377738-3777749.
12. Utyushev A.D., Zakomirnyi V.I., and Rasskazov I.L. Collective lattice resonances: Plasmonics and beyond. Reviews in Physics **2021**, 6 100051-100072.
13. Shi Y., Dong Y., Sun D., and Li G. Significant Near-Field Enhancement over Large Volumes around Metal Nanorods via Strong Coupling of Surface Lattice Resonances and Fabry–Pérot Resonance. Materials, **2022**, 15 1523-1535.
14. Cherqui C., Bourgeois M.R., Wang D., and C. Schatz G.C. Plasmonic Surface Lattice Resonances: Theory and Computation. Acc. Chem. Res. **2019**, 52 2548-2558.
15. Tellez-Limon R., Gardillou F., Coello V. and Salas-Montiel R. Coupled localized surface plasmon resonances in periodic arrays of gold nanowires on ion-exchange waveguide technology. J. Opt. **2021**, 23 025801-0258110.
16. Yang T and Crozier B.K. Dispersion and extinction of surface plasmons in an array of gold nanoparticle chains: influence of the air/glass interface. Optics Express. **2008**, 12 8750-8580.
17. Bin-Alam M.S., Reshef O., Mamchur, Zahirul Alam Y.M., Carlow G., Upham J., Sullivan B.T., Ménard J-M, Huttunen M.J., Boyd R.W., and Dolgaleva K. Ultra-high-Q resonances in plasmonic metasurfaces. Nature Comm. **2021**, 12 1-8.
18. Garcia-Ortiz C.E., Cortes R., Gomez-Correa J.E., Pisano, J. Fiutowski J., Garcia-Ortiz, Ruiz-Cortes V., Rubahn H—G., and Coello V. Plasmonic metasurface Luneburg lens Photonics Research. **2019** 7, 1112-1118.
19. Foteinopoulou S., Vigneron J.P., and Vandenbem C. Optical near-field excitations on plasmonic nanoparticle-based structures.
20. Giannini V., Fernández-Domínguez A.I., Heck S.C., and Maier S.A. Plasmonic Nanoantennas: Fundamentals and Their Use in Controlling the Radiative Properties of Nanoemitters. Chem. Rev. **2011**, 111 3888-3912.
21. Coello V., Bozhevolnyi S.I. Surface plasmon polariton excitation and manipulation by nanoparticle arrays. Optics Communications **2009** 282, 3032-3036.
22. Pisano E., Coello V., Garcia-Ortiz C.E., Chen Y., Beermann J., and I. Bozhevolnyi S.I. Plasmonic channel waveguides in random arrays of metallic nanoparticles. Optics Express **2016**, 24 17080-17089.
23. He Y., Boxiang Song B., and Tang J. Optical metalenses: fundamentals, dispersion manipulation, and applications. Frontiers of Optoelectronics **2022**, 15 1-31.

24. Koenderink A.F. Plasmon Nanocavity Array Lasers: Cooperating over Losses and Competing for Gain. ACS Nano **2019**, 13, 7377-7382.
25. Pors A., and Bozhevolnyi S.I. Gap plasmon-based phase-amplitude metasurfaces: material constraints. Opt. Mat. Exp. **2015**, 11 2448-2458.
26. Yamada H., Kawasaki D., Sueyoshi K., Hisamoto H., and Endo T. Fabrication of Metal-Insulator-Metal Nanostructures Composed of Au-MgF2-Au and Its Potential in Responding to Two Different Factors in Sample Solutions Using Individual Plasmon Modes. Micromachines. **2022**, 13 257-269.
27. Aalizadeh M., Khavasi A., Butun B., and Ozba E. Large-Area, Cost-Effective, Ultra-Broadband Perfect Absorber Utilizing Manganese in Metal-Insulator-Metal Structure. Sci. Rep. **2018**, 8 9162-9174.
28. Ding F., A Review of Multifunctional Optical Gap-Surface Plasmon Metasurfaces. Progress In Electromagnetics Research **2022**, 174 55-73.
29. Naresh V and Lee N. A Review on Biosensors and Recent Development of Nanostructured Materials-Enabled Biosensors. Sensors **2021**, 21 1109-1143.
30. Boyd R.W. *Nonlinear Optics*, 4th ed.; Academic Press, USA, **2020**, pp. 1-634.
31. Ana Isabel Perez-Jimenez A.P., Lyu D., Lu Z., Guokun Liu G., and Ren B. Surface-enhanced Raman spectroscopy: benefits, trade-offs and future developments. Chem. Sci. **2020**, 11 4563-4577.
32. Johnson P.B. and Christy R.W. Optical Constants of the Noble Metals. Phys. Rev. B. **1972** 6 4370-4379.
33. Palik E.D. Handbook of Optical Constants of Solids. Academic Press, USA, **1998**, 1-999.
34. Hohenau A., Krenn J., Garcia-Vidal F., Rodrigo S., Martin-Moreno L., Beermann J., and Bozhevolnyi S. Spectroscopy and nonlinear microscopy of gold nanoparticle arrays on gold films. Phys. Rev. B **2007**, 75 085104-085111.
35. Wood R.W. On a Remarkable Case of Uneven Distribution of Light in a Diffraction Grating Spectrum. Proc. Phys. Soc. London **1902,** 18 269-275.